2023

Efficient 2075-nm Laser Emission From Ho3+-Doped Fluorotellurite Glass in a Compact All-Fiber Structure

Liyuan Wang
Harbin Engineering University, Harbin, China

Xiaotong Zhao
Harbin Engineering University, China

Nian Lv
Harbin Engineering University, China

See next page for additional authors

Funder: National Natural Science Foundation of China; Natural Science Foundation of Heilongjiang Province; Shenzhen Basic Research Project, Heilongjiang Touyan Innovation Team Program; Fundamental Research Funds for the Central Universities

To be published in Optics Letters:

Title: Efficient 2075 nm laser emission from Ho3+-doped fluorotellurite glass in a compact all-fiber structure

Authors: Liyuan Wang,Xiaotong Zhao,Nian Lv,NianNian Xu,zhenrui Li,Gerald Farrell,Shunbin Wang,Pengfei Wang

Accepted: 06 April 23

Posted 06 April 23

DOI: https://doi.org/10.1364/OL.488256

Efficient 2075 nm laser emission from Ho^{3+}-doped fluorotellurite glass in a compact all-fiber structure

LIYUAN WANG,[1] XIAOTONG ZHAO,[1] NIAN LV,[1] NIANNIAN XU,[1] ZHENRUI LI,[1] GERALD FARRELL[3], SHUNBIN WANG,[1,4] AND PENGFEI WANG[1,2,5]

[1]*Key Laboratory of In-Fiber Integrated Optics, Ministry Education of China, Harbin Engineering University, Harbin 150001, China*
[2]*Key Laboratory of Optoelectronic Devices and Systems of Ministry of Education and Guangdong Province, College of Optoelectronic Engineering, Shenzhen University, Shenzhen, 518060, China*
[3]*Photonics Research Center, Technological University Dublin, Grangegorman Campus, Dublin 7, Ireland*
[4]*e-mail: shunbinwang@hrbeu.edu.cn*
[5]e-mail: *pengfei.wang@tudublin.ie*

In this letter, we report a Ho^{3+}-doped fluorotellurite glass all-fiber laser at 2075 nm. The gain fiber is pumped in-band with a 1976 nm fiber laser and connected by fusion splicing. A high-quality fusion splicing point with a loss of < 0.1 dB was obtained by finely adjusting the splicing power and offset. In addition, by optimizing the writing parameters, a third-order fiber Bragg grating (FBG) with a reflectivity of 98% was achieved at 2075 nm using the femtosecond laser direct-writing method. Using the FBG as the laser cavity mirror and a relatively short 28-cm-long home-made Ho^{3+}-doped fluorotellurite fiber as the laser medium, a laser with a maximum unsaturated output power of 7.33 W was obtained, and the corresponding slope efficiency was as high as 93.4%. The first demonstration of the fluorotellurite glass all-fiber ~2.1 μm laser presented in this work may pave the way for a high-power 2.1 μm fiber laser with a compact structure.

http://dx.doi.org/99.9999/OL.99.099999

~2.1 μm fiber lasers have attracted tremendous attention due to their wide applications in optical communication, lidar, medical diagnosis and treatment, atmospheric sensing, photoelectric countermeasures, pollution monitoring, and the generation of mid-infrared light sources [1-6]. Currently, ~2.1 μm fiber lasers have been achieved in silica, silicate, fluoride, tellurite, and germanate glass fibers. Tellurite glass is a desirable gain matrix for fiber lasers because of its low phonon energy, a high doping concentration of rare earth ions, excellent stability, and good fiber formation [7]. In 2008, Tsang *et al.* used a 1.6 μm fiber laser to pump Tm^{3+}/Ho^{3+} codoped tellurite fiber and obtained a ~2.1 μm laser with a slope efficiency of 62% [8]. In the same year, they achieved a ~2.1 μm laser output with a slope efficiency of 25% by pumping a $Yb^{3+}/Tm^{3+}/Ho^{3+}$ triple-doped tellurite fiber with a 1.1 μm fiber laser [9]. In 2015, Yao *et al.* demonstrated a ~2.1 μm laser in a 27 cm long Ho^{3+}-doped fluorotellurite microstructure fiber (FTMF), and the unsaturated maximum power was 161 mW, corresponding to a slope efficiency of 67.4% [10]. In 2016, Yao *et al.* employed an 1120 nm fiber laser to pump a 42 cm long Ho^{3+}-doped FTMF and obtained ~2.1 μm unsaturated maximum power of 98 mW with a slope efficiency of 12.4% [11]. In 2019, Zhao *et al.* used a 1980 nm fiber laser to pump a 30 cm long Ho^{3+}-doped FTMF and obtained a ~2.1 μm laser with an unsaturated maximum output power of 8.08 W and a slope efficiency of 77.21% [12]. The above ~2.1 μm lasing using fluorotellurite fibers was achieved based on a spatially coupled cavity, which has drawbacks such as low coupling efficiency, poor stability, and low integration. It is necessary to develop an all-fiber cavity structure using fiber Bragg gratings (FBGs) and fusion splicing for heterogeneous fibers to improve the laser's stability and integration.

The employment of FBGs in the field of fiber lasers is prevalent due to their benefits of low insertion loss, good fiber compatibility, and specific wavelength selection. In 2009, Bernier *et al.* prepared an FBG with a reflectivity of 95% in ZBLAN double-clad fiber. They built a mid-infrared all-fiber laser with the FBG as a high reflector, obtaining a laser output power of 5 W and an optical-to-optical conversion efficiency of 32% [13]. In 2015, Fortin *et al.* developed a high-reflectivity fiber Bragg grating (HR-FBG) and a low-reflectivity FBG. They obtained a continuous laser output power of up to 30.5 W at 2.94 μm with an overall laser efficiency of 16% [14]. In 2019, Fortin *et al.* inscribed FBGs in Dy-doped ZBLAN fiber and achieved a 3.24 μm laser output with a slope efficiency of 58% and an output power of 10.1 W [15].

In 2021, Liu *et al.* inscribed fluorotellurite FBGs at the wavelength of 1553 nm in TeO_2-ZnF_2-NaF glass fibers [16]. However, until now, FBGs written in fluorotellurite fiber have yet to be studied for lasing. In this letter, we prepared FBGs at a central wavelength of 2075 nm in Ho^{3+}-doped fluorotellurite fibers using the femtosecond (fs) laser direct writing method. The properties of FBGs under different pulse energies, grating orders, and grating lengths were investigated in detail. In addition, a high-quality fusion-splicing point was obtained with an insertion loss of < 0.1 dB by finely adjusting the splicing power and offset. By using an HR-FBG as a high reflector and low-loss splicing point to connect pump output fiber and gain fiber, we

achieved an all-fiber laser at 2075 nm in fluorotellurite fibers for the first time, to the best of our knowledge, the laser efficiency was as high as 93.4% and the maximum unsaturated output power was 7.33 W (limited by the pump output power).

The fluorotellurite fiber we used is fabricated by using the rod-in-tube method. The composition of the core was $65TeO_2$-$10BaF_2$-$10ZnF_2$-$9.25Y_2O_3$-$5Al_2O_3$-$0.75Ho_2O_3$ (mol%). The fiber has a core diameter of 11.5 μm and a cladding diameter of 240 μm. The fiber's numerical aperture (NA) at 2.1 μm was about 0.29. The background loss of the fiber was estimated to be ~0.8 dB/m at λ ~1570 nm using a cut-back method [17]. The silica fiber (Corning, SMF-28) has a core diameter of 8.3 μm and a cladding diameter of 125 μm. The equipment required for the experiment includes a fiber splicer (Thorlabs, GPX-3400), a cleaver (Thorlabs, LDC401A), a fs laser (Solstice Ace), an optical spectrum analyzer (OSA, Yokogawa AQ6375B), a 1570 nm laser (FL-1570-2000-B), a home-made 1976 nm laser, an assembled supercontinuum source (SC), an optical microscope (Nikon, LV100N), and a power meter (Thorlabs S470C).

The filament fusion splicing is schematically illustrated in Fig. 1(a). The filament is an inverted Ω shape, and the material is iridium. Iridium filament can heat fibers at low temperatures, forming a uniform and stable temperature field for working with soft glass fibers. Due to the difference in glass transition temperature between fluorotellurite glass fiber (Tg ~425 °C) and silica fiber (Tg ~1215 °C) [18], the asymmetric fusion splicing method is adopted for the fusion splicing. The filament offset is not zero, and the filament's position is biased toward the silica fiber. The heating temperature should be lower than the softening temperature of the silica fiber and higher than the softening temperature of the fluorotellurite glass fiber. During the fusion splicing process, the fiber end with a low softening temperature gets molten, then the fiber with a high softening temperature is inserted and wrapped.

We investigated the insertion loss and mechanical strength of the fusion splicing point to characterize its performance of the fusion splicing point. The method used to measure the loss of the fusion splicing point is the cut-back method. The 1570 nm laser is utilized as a test source and is injected into the fluorotellurite fiber. The loss of the fusion splicing point could be calculated by measuring the attenuation of the 1570 nm laser source through the fusion splicing point. The loss of the fusion splicing point is calculated as $\delta=10\lg P_{in}-10\lg P_{out}-\alpha L$, where P_{in} and P_{out} are the laser power of the tested source and the output power of fluorotellurite fiber, respectively, L is the length of the fluorotellurite fiber, and α is the attenuation of the fluorotellurite fiber [19].

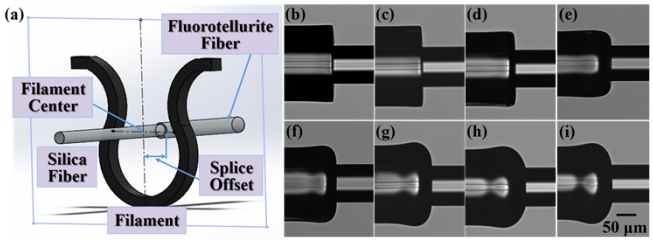

Fig. 1. (a). Schematic of the filament fusion splicing. (b-i). Fluorotellurite fiber and silica fiber splicing point pictures under different fusion splicing power (b: 9.0 W; c: 9.1 W; d: 9.2 W; e: 9.3 W; f: 9.4 W; g:9.5 W; h: 9.6 W; i:9.7 W).

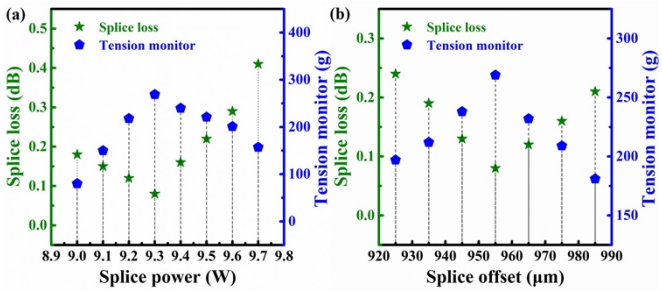

Fig. 2. (a). Effect of fusion splicing power on fusion splicing loss and monitored tension. (b). Effect of fusion splicing offset on fusion splicing loss and monitored tension.

The shape of the fusion splicing point is essential to judge its performance. Among the fusion splicing parameters, fusion splicing power is crucial to the fusion splicing point. Fig. 1(b)–(i) shows the shape of the fusion splicing point between the fluorotellurite and silica fibers with different fusion splicing powers (9.0 W to 9.7 W). As shown in Fig. 1(b)–(d), when the fusion splicing power is low, the fluorotellurite and silica fiber cannot be fused together sufficiently, and the mechanical strength of the fusion splicing point is weak. In addition, as shown in Fig. 1(f)–(i), the loss of the splicing point significantly increased with high fusion splicing power as it deformed the fluorotellurite fiber. As shown in Fig. 2(a), we investigated the splice loss changes and tensile force as the splice power increased. At the same fusion splicing power of 9.3 W, the turning points in the variations in splicing loss and tensile force are indicated. When the power is changed from 9.0 W to 9.3 W, the splicing loss decreases from 0.18 dB to 0.08 dB, while the tensile force increases from 80 to 269 g. The splicing loss is increased from 0.08 dB to 0.41 dB when the fusion splicing power varies from 9.3 W to 9.7 W and the tensile force is decreased from 269 g to 157 g. The outcome indicates that 9.3 W is the ideal fusion splicing power.

It was discovered that the splice offset significantly impacts mechanical strength. In order to optimize the performance of the fusion splicing point, we study the splicing loss and tensile force of the fusion splicing points at different splice offset distances. Fig. 2(b) shows the variation of the splicing loss and tensile force with splice offset. When the splice offset varies from 925 to 955 μm, the splicing loss decreases from 0.24 dB to 0.08 dB, while the tensile force increases from 197 to 269 g. The splicing loss increases, and the tensile force decreases as the splice offset changes from 955 to 985 μm. The proper splice offset is 955 μm, as can be found.

A schematic of the fs laser direct writing system employed for the fabrication of the FBG is illustrated in Fig. 3. The fs laser has a central wavelength of 800 nm, a repetition frequency of 1 kHz, and a pulse duration of 100 fs. The fs laser beam was focused into the fluorotellurite fiber sample using an objective lens (40×, NA 0.65, Olympus). The fiber was placed between a glass slide and coverslip and fixed on the high-precision 3D platform (Newport Corp.) through the clamps. In order to reduce the aberration caused by the cylindrical surface and high refractive index of the fluorotellurite fiber, a refractive index-matching liquid (n = 1.780) was added between the glass slide and the coverslip. A computer can precisely control the fs laser pulse energy and the movement of the 3D platform. The CCD can observe the fs laser beam focusing on the fiber. This work used an fs laser line-by-line direct writing method to fabricate the FBGs. The schematic diagram of the line-by-line direct writing method of FBG is presented in Fig. 3(b). Each grating

was inscribed at a distance of l (transversal length) by moving the fiber relative to the focus of the laser beam. The grating period (Λ) is defined as the spacing between two lines, and the phase matching condition for the Bragg resonance wavelength (λ_B) can be determined by $2n_{eff}\Lambda/m$, where m is the order of the FBG and n_{eff} is the refractive index of the fiber core at the reflection wavelength. The reflectivity (R) can be calculated as R=1-10$^{(-T/10)}$, where T is the absolute depth of the transmission dip in decibels (dB) at λ_B.

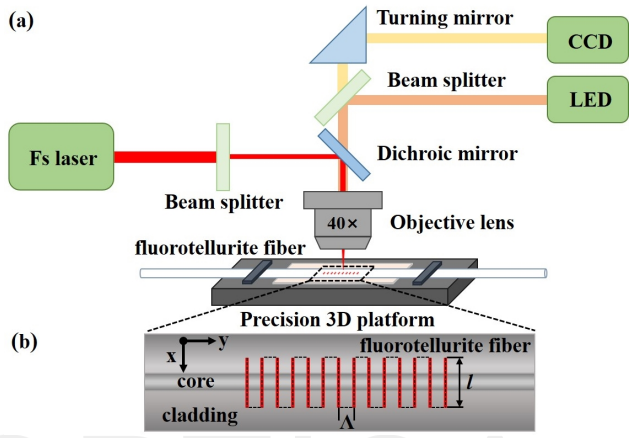

Fig. 3. (a). Fs laser writing system schematic for the fabrication of the FBG. (b). Schematic diagram of the line-by-line direct writing method of FBG.

The transmission spectra of FBGs were measured and recorded using an assembled SC (1.9–4.0 μm) and an OSA (AQ6375B) with a resolution of 0.05 nm and a measurement range of 1200–2400 nm. The transmission spectra of FBGs inscribed at different pulse energies (Ep) are shown in Fig. 4(a). The corresponding microscope images of the top view, side view, and cross-section are illustrated in Fig. 4(b)–(d), (e)–(g), and (h)–(j), respectively. A series of third-order FBGs with Λ ~1.71 μm and λ_B ~2075 nm were written for three different Ep values of ~0.15 μJ, 0.30 μJ, and 0.45 μJ, respectively. The inscription length and inscription speed of the FBGs were 10 mm and 60 μm/s, respectively. When the Ep increased from 0.15 to 0.45 μJ, the R of the FBG increased from 92% to 98% and then decreased to 95.4%. When Ep was 0.15 μJ, the grating planes were barely visible, as shown in Fig. 4(b). The refractive index modification covers the core of the fluorotellurite fiber, as seen in Fig. 4(i) and (j). This results in a 100% modal overlap [20], which considerably raises the R of the FBG. However, when Ep was increased to 0.45 μJ, apparent damage appeared in the fiber [see Fig. 4(j)], which caused a decrease in R. To summarize, the fluorotellurite fiber grating is incredibly susceptible to the writing laser pulse energy. As we can see from Fig. 4(a), with the increase in Ep, the insertion loss of the grating increases from 0.45 dB/cm to 0.68 dB/cm to 0.79 dB/cm.

Since Ep~0.3 μJ provided the highest R, this Ep value was used to study the relationship between m and R. The Ep, speed, and length of the FBGs were 0.3 μJ, 60 μm/s, and 10 mm, respectively. For m = 3, 4, and 5, the Λ values were 1.71 μm, 2.28 μm, and 2.85 μm, respectively. We did not inscribe the first- and second-order gratings to avoid overlapping grating planes. In Fig. 5(a), the third-order grating has the most significant resonance dip, as is apparent. It displays the Bragg resonance at 2075 nm with a transmission dip of 17 dB, R = 98%, a 3-dB bandwidth of 0.76 nm, and an insertion loss of 0.68 dB/cm. The transmission dip for m = 4 and 5 is 13.2 dB (R = 95.2%) and 11.6 dB (R = 93%). It can be explained that a consistent drop in R results from the number of grating planes for a fixed FBG length decreasing with increasing order. The 3-dB bandwidths of the fourth- and fifth-order FBGs are 0.60 nm and 0.54 nm, respectively. The R of the fiber grating is also related to the length of the grating. As shown in Fig. 5(b), the transmission dip of FBG increases gradually with increasing length. The resonance dips of 5, 7, and 10 mm are 11.3 dB (R = 92.6%), 13.7 dB (R = 95.7%), and 17 dB (R = 98%), respectively. Since more grating planes are in a more extended grating, it has a higher R.

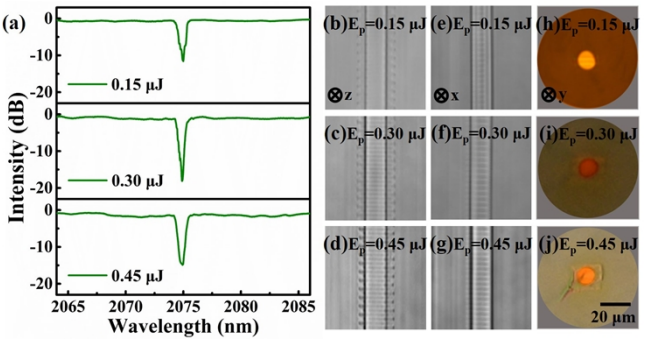

Fig. 4. (a). Transmission spectra of the FBGs at different pulse energies. (b-j). Microscope images of the FBGs at different pulse energies (b-d: top view; e-g: side view; h-j: cross-sectional image).

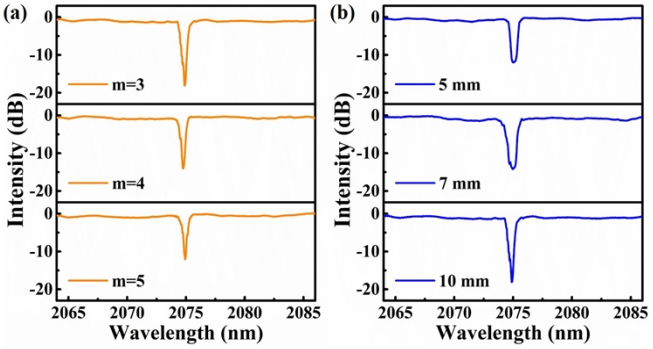

Fig. 5. (a). Transmission spectra of the FBGs with different orders. (b). Transmission spectra of the FBGs with different grating lengths.

The fiber laser schematic is shown in Fig. 6. A 1976 nm fiber laser was used as the pump source, with a maximum output power of 8.46 W. Ho^{3+}-doped fluorotellurite fibers were used as the gain medium. Fusion splicing is used to inject the pump light into the fluorotellurite fiber. The loss of the fusion splicing point is 0.08 dB. A HR-FBG (R = 98%) is etched into one end of the fiber. The other end utilizes Fresnel reflection (~9% at 2075 nm) on the fiber end face so that the Ho^{3+}-doped fluorotellurite fiber can form a laser cavity. The output end of the fiber was mechanically spliced to a large mode area fluoride cable to connect the OSA (AQ6375B) and monitor the spectrum of output light from the Ho^{3+}-doped fluorotellurite fiber. The power meter measures the output power of the Ho^{3+}-doped fluorotellurite fiber.

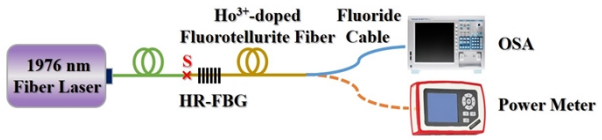

Fig. 6. Schematic diagram of the 2075 nm laser experimental setup. The label S identifies the fusion splice point.

Fig. 7(a) depicts the relationship between the launched pump power and the 2.1 μm laser output power. When the pump power was increased to 56 mW, lasing at 2075 nm was observed. The unsaturated output power of the 2075 nm laser rose monotonically with the increase in pump power. When the pump power was 8.46 W, the maximum output power was 7.33 W (limited by the pump output power), and the slope efficiency was 93.4%. Fig. 7(b) shows the output spectrum of the laser for a launched pump power of 8.46 W. The FWHM bandwidth of the laser line was estimated to be approximately 0.072 nm.

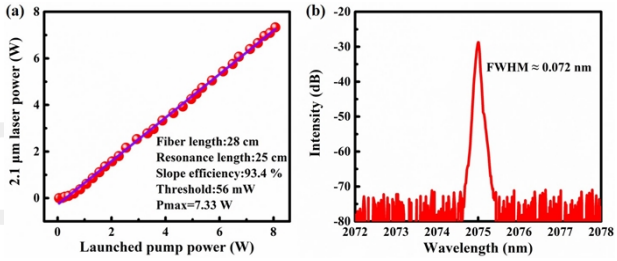

Fig. 7. (a). Output power of the 2075 nm laser as a function of the launched pump power at 1976 nm. (b). Output spectrum of the laser at a launched pump power of 8.46 W.

The dependence of slope efficiency and lasing threshold on resonance length was measured to study the effect of resonance length on laser performance, as shown in Fig. 8. The slope efficiency increased from 74.49% to 93.4% with a resonance length increase from 11 to 25 cm, and the lasing threshold first rose from 53 to 71 mW (~20 cm) before falling to 56 mW. The slope efficiency fell from 93.4% to 66.73% as the resonance length was extended from 25 to 43 cm, while the lasing threshold rose from 56 to 110 mW. Therefore, 25 cm was the optimal resonance length for producing highly effective, low-threshold lasers.

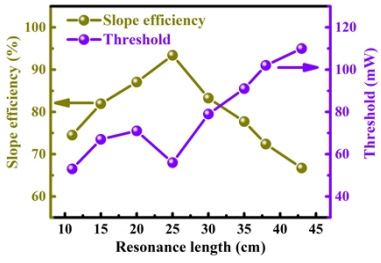

Fig. 8. Effect of resonance length on slope efficiency and threshold.

In conclusion, our results demonstrate the successful development of a compact, all-fiber structure Ho^{3+}-doped fluorotellurite glass laser operating at a wavelength of 2075 nm. The laser used a third-order HR-FBG and low-loss fusion splice to launch the pump beam in the home-made Ho^{3+}-doped fluorotellurite fiber. The laser showed a high efficiency of 93.4% and stable operation with a narrow linewidth of 0.072 nm, which makes it a promising candidate for various applications such as medical treatment, remote sensing, and optical communications. The simple and low-cost fabrication process of the all-fiber structure also provides potential for mass production and commercialization of this compact fiber laser system.

Funding. National Natural Science Foundation of China (61905048, 61935006, 62005060, 62005061, 62090062); Natural Science Foundation of Heilongjiang Province (LH2020F030); National Key Research and Development Program of China (2020YFA0607602); Shenzhen Basic Research Project (JCYJ20190808140805488, JCYJ20190808173619062); 111 Project (B13015); Heilongjiang Touyan Innovation Team Program; Fundamental Research Funds for the Central Universities (3072022TS2612).

Disclosures. The authors declare no conflicts of intertest.

Data availability. Data underlying the results presented in this paper are not publicly available at this time but may be obtained from the authors upon reasonable request.

References

1. B. Guo, Y. Wang, C. Peng, H. Zhang, G. Luo, H. Le, C. Gmachl, D. L. Sivco, M. L. Peabody, and A.Y. Cho, Opt. Express **12**, 208 (2004).
2. J.-P. Cariou, B. Augere, and M. Valla, C. R. Physique **7**, 213 (2006).
3. A. Hemming, N. Simakov, J. Haub, and A. Carter, Opt. Fiber Technol. **20**, 621 (2014).
4. F. Lou, P.-W. Kuan, L. Zhang, S. Wang, Q. Zhou, M. Wang, S. Feng, K. Li, C. Yu, and L. Hu, Opt. Mater. Express **4**,1267 (2014).
5. W. Shi, Q. Fang, X. Zhu, R. A. Norwood, and N. Peyghambarian, Appl. Opt. **53**, 6554 (2014).
6. D. G. Lancaster and S. D. Jackson, Opt. Lett. **34**, 3412 (2009).
7. V. V. R. K. Kumar, A. K. George, J. C. Knight, and P. St. J. Russell, Opt. Express **11**, 2641 (2003).
8. Y. Tsang, B. Richards, D. Binks, J. Lousteau, and A. Jha, Opt. Lett. **33**, 1282 (2008).
9. Y. Tsang, B. Richards, D. Binks, J. Lousteau, and A. Jha, Opt. Express **16**, 10690 (2008).
10. C. Yao, C. He, Z. Jia, S. Wang, G. Qin, Y. Ohishi, and W. Qin, Opt. Lett. **40**, 4695 (2015).
11. C. Yao, Z. Jia, C. He, S. Wang, L. Zhang, Y. Feng, Y. Ohishi, G. Qin, and W. Qin, IEEE Photonics Technol. Lett. **28**, 1084 (2016).
12. Z. Zhao, C. Yao, Z. Li, Z. Jia, G. Qin, Y. Ohishi, and W. Qin, Laser Phys. Lett. **16**, 115101 (2019).
13. M. Bernier, D. Faucher, N. Caron, and R. Vallée, Opt. Express **17**, 16941 (2009).
14. V. Fortin, M. Bernier, S. T. Bah, and R. Vallée, Opt. Lett. **40**, 2882 (2015).
15. V. Fortin, F. Jobin, M. Larose, M. Bernier, and R. Vallée, Opt. Lett. **44**, 491 (2019).
16. L. Liu, F. Chen, X. Xiao, X. Li, R. Wang, C. Liu, and H. Guo, Opt. Lett. **46**, 4832 (2021).
17. M. Frank, M. Jelínek, V. Kubeček, I. Kašík, O. Podrazký, and V. Matějec, J. Lightwave Technol. **36**, 2271 (2018).
18. K. Yin, B. Zhang, J. Yao, L. Yang, S. Chen, and J. Hou, Opt. Lett. **41**, 946 (2016).
19. L. Yang, Y. Wang, K. Jiao, S. Dai, R. Zhao, Q. Nie, X. Wang, Z. Jia, G. Qin, Infrared Physics and Technology **122**, 104075 (2022).
20. M. Ams, P. Dekker, S. Gross, and M. J. Withford, Nanophotonics **6**, 743 (2017).

Full citation listings

[1] B. Guo, Y. Wang, C. Peng, H. Zhang, G. Luo, H. Le, C. Gmachl, D. L. Sivco, M. L. Peabody, and A.Y. Cho, "Laser-based mid-infrared reflectance imaging of biological tissues," Opt. Express 12, 208 (2004).

[2] J.-P. Cariou, B. Augere, and M. Valla, "Laser source requirements for coherent lidars based on fiber technology," C. R. Physique 7, 213 (2006).

[3] A. Hemming, N. Simakov, J. Haub, and A. Carter, "A review of recent progress in holmium-doped silica fibre sources," Opt. Fiber Technol. 20, 621 (2014).

[4] F. Lou, P.-W. Kuan, L. Zhang, S. Wang, Q. Zhou, M. Wang, S. Feng, K. Li, C. Yu, and L. Hu, "2 μm laser properties of Tm^{3+}-doped large core sol-gel silica fiber," Opt. Mater. Express 4,1267 (2014).

[5] W. Shi, Q. Fang, X. Zhu, R. A. Norwood, and N. Peyghambarian, "Fiber lasers and their applications [Invited]," Appl. Opt. 53, 6554 (2014).

[6] D. G. Lancaster and S. D. Jackson, "In-fiber resonantly pumped Q-switched holmium fiber laser," Opt. Lett. 34, 3412 (2009).

[7] V. V. R. K. Kumar, A. K. George, J. C. Knight, and P. St. J. Russell, "Tellurite photonic crystal fiber," Opt. Express 11, 2641 (2003).

[8] Y. Tsang, B. Richards, D. Binks, J. Lousteau, and A. Jha, "Tm^{3+}/Ho^{3+} codoped tellurite fiber laser," Opt. Lett. 33, 1282 (2008).

[9] Y. Tsang, B. Richards, D. Binks, J. Lousteau, and A. Jha, "A Yb^{3+}/Tm^{3+}/Ho^{3+} triply-doped tellurite fibre laser," Opt. Express 16, 10690 (2008).

[10] C. Yao, C. He, Z. Jia, S. Wang, G. Qin, Y. Ohishi, and W. Qin, "Holmium-doped fluorotellurite microstructured fibers for 2.1 μm lasing," Opt. Lett. 40, 4695 (2015).

[11] C. Yao, Z. Jia, C. He, S. Wang, L. Zhang, Y. Feng, Y. Ohishi, G. Qin, and W. Qin, "2.074 μm lasing from Ho^{3+}-doped fluorotellurite microstructured fibers pumped by a 1120 nm laser," IEEE Photonics Technol. Lett. 28, 1084 (2016).

[12] Z. Zhao, C. Yao, Z. Li, Z. Jia, G. Qin, Y. Ohishi, and W. Qin, "8.08 W holmium-doped fluorotellurite fiber laser at 2067 nm," Laser Phys. Lett. 16, 115101 (2019).

[13] M. Bernier, D. Faucher, N. Caron, and R. Vallée, "Highly stable and efficient erbium-doped 2.8 μm all fiber laser," Opt. Express 17, 16941 (2009).

[14] V. Fortin, M. Bernier, S. T. Bah, and R. Vallée, "30 W fluoride glass all-fiber laser at 2.94 μm," Opt. Lett. 40, 2882 (2015).

[15] V. Fortin, F. Jobin, M. Larose, M. Bernier, and R. Vallée, "10-W-level monolithic dysprosium-doped fiber laser at 3.24 μm," Opt. Lett. 44, 491 (2019).

[16] L. Liu, F. Chen, X. Xiao, X. Li, R. Wang, C. Liu, and H. Guo, "Direct femtosecond laser inscription of an IR fluorotellurite fiber Bragg grating," Opt. Lett. 46, 4832 (2021).

[17] M. Frank, M. Jelínek, V. Kubeček, I. Kašík, O. Podrazký, and V. Matějec, "Scanning Cutback Method for Characterization of Bragg Fibers," J. Lightwave Technol. 36, 2271 (2018).

[18] K. Yin, B. Zhang, J. Yao, L. Yang, S. Chen, and J. Hou, "Highly stable, monolithic, single-mode mid-infrared supercontinuum source based on low-loss fusion spliced silica and fluoride fibers," Opt. Lett. 41, 946 (2016).

[19] L. Yang, Y. Wang, K. Jiao, S. Dai, R. Zhao, Q. Nie, X. Wang, Z. Jia, G. Qin, "High-coupling efficiency and robust fusion splicing between fluorotellurite and chalcogenide fibers," Infrared Physics and Technology 122, 104075 (2022).

[20] M. Ams, P. Dekker, S. Gross, and M. J. Withford, "Fabricating waveguide Bragg gratings (WBGs) in bulk materials using ultrashort laser pulses," Nanophotonics 6, 743 (2017).